Electron Exchange and the Photophysics of Metal−Quinone Complexes. 1. Synthesis and Spectroscopy of Chromium−Quinone Dyads

Daniel E. Wheeler and James K. McCusker*

Department of Chemistry, University of California at Berkeley, Berkeley, California 94720-1460

Received October 16, 1997

The synthesis, structural and spectroscopic characterization of monosemiquinone and monocatechol complexes of chromium(III) are described. Compounds of the general form $[Cr(N_4)Q]^{n+}$, where N_4 represents a tetradentate or bis-bidentate nitrogenous ligand or ligands and Q represents a reduced form of an orthoquinone, have been prepared by two different routes from Cr^{III} and Cr^{II} starting materials. The complex [Cr(tren)(3,6-DTBSQ)]-$(PF_6)_2$, where tren is tris(2-aminoethyl)amine and 3,6-DTBSQ is 3,6-di-*tert*-butylorthosemiquinone, crystallizes in the monoclinic space group $P2_1/c$ with $a = 11.9560(2)$ Å, $b = 17.0715(4)$ Å, $c = 17.1805(4)$ Å, $\beta = 90.167(1)°$, $V = 3506.6(1)$ Å^3, $Z = 4$, with $R = 0.056$ and $R_w = 0.070$. Alternating C−C bond distances within the quinoidal ligand confirm its semiquinone character. Variable temperature magnetic susceptibility data collected on solid samples of both [Cr(tren)(3,6-DTBSQ)]$(PF_6)_2$ and [Cr(tren)(3,6-DTBCat)](PF_6) in the range 5−350 K exhibit temperature-independent values of $2.85 \pm 0.1\ \mu_B$ and $3.85 \pm 0.1\ \mu_B$, respectively. These data are consistent with a simple Cr^{III}−catechol formulation ($S = {}^3/_2$) in the case of [Cr(tren)(3,6-DTBCat)](PF_6) and strong antiferromagnetic coupling ($|J| > 350$ cm^{-1}) between the Cr^{III} and the semiquinone radical in [Cr(tren)(3,6-DTBSQ)]-$(PF_6)_2$. The absorption spectrum of the semiquinone complex exhibits a number of sharp, relatively intense transitions in fluid solution. Group theoretical arguments coupled with a qualitative ligand-field analysis including the effects of Heisenberg spin exchange suggest that several of the observed transitions are a consequence of exchange interactions in both the ground- and excited-state manifolds of the compound. The effect of electron exchange on excited-state dynamics has also been probed through static emission as well as time-resolved emission and absorption spectroscopies. It is suggested that the introduction of exchange coupling and subsequent change in the molecule's electronic structure may contribute to an increase of nearly 4 orders of magnitude in the rate of radiative decay (k_r), and a factor of ca. 10^7 in the rate of nonradiative decay (k_{nr}).

Introduction

The study of electron exchange interactions in transition metal complexes has historically represented an active area of research in inorganic chemistry.[1−9] Most of the earlier work on electron exchange focused on establishing correlations between the nature and magnitude of electron exchange with molecular structure, identification of orbital exchange pathways, etc.[9] These efforts have brought the field of magnetochemistry to a point where researchers are able to understand and predict with reasonable certainty the magnetic properties of simple, coupled systems. Although the relevance of exchange interactions to areas of chemistry both within and outside of the inorganic community has always been clear,[10] the field is still considered by many to be somewhat specialized. However, interest in exchange coupling is now expanding from its origins in fundamental electronic structure research to encompass a variety of disciplines ranging from biology to materials science. For example, the present flurry of activity aimed at developing true molecular-based materials has fueled a resurgence in research efforts aimed at understanding the electronic structure of more complex systems. Characterization of "molecular magnets",[11−16] spin frustration effects,[17−20] and the development of organic-based

(1) O'Conner, C. J. *Research Frontiers in Magnetochemistry*; O'Conner, C. J., Ed.; World Scientific Publishing Co. Pte. Ltd.: Singapore, 1993.
(2) Griffith, J. S. *Struct. Bonding (Berlin)* **1972**, *10*, 87.
(3) Carlin, R. L. *Coord. Chem. Rev.* **1987**, *79*, 215.
(4) Hodgson, D. J. *J. Mol. Catal.* **1984**, *23*, 219.
(5) Bencini, A.; Gatteschi, D. *EPR of Exchange-Coupled Systems*; Springer-Verlag: Berlin, 1990.
(6) *Properties of Magnetically Condensed Systems*; Hatfield, W. E., Ed.; John Wiley and Sons: New York, 1976.
(7) Tsukerblat, B. S.; Belinskii, M. I.; Fainzil'berg, V. E. *Sov. Sci. Rev., Sect. B.* **1987**, *9*, 337.
(8) O'Conner, C. J. *Prog. Inorg. Chem.* **1982**, *29*, 203.
(9) Kahn, O. *Molecular Magnetism*; VCH Publishers: New York, 1993.
(10) For example, the antiferromagnetic part of the exchange interaction matrix in a Tanabe exchange formalism can be mathematically related to a one-electron transfer integral between the coupled magnetic orbitals. See ref 29 for further details.
(11) *Magnetic Molecular Materials*; Gatteschi, D., Kahn, O., Miller, J. S., Palacio, F., Eds.; Kluwer Academic Publishers: Dordrecht, The Netherlands, 1991; Vol. 198.
(12) *Molecular Inorganic Magnetic Materials*; Kahn, O., Pei, Y., Journaux, Y., Eds.; Wiley and Sons: New York, 1992.
(13) Sessoli, R.; Tsai, H. L.; Schake, A. R.; Wang, S. Y.; Vincent, J. B.; Folting, K.; Gatteschi, D.; Christou, G.; Hendrickson, D. N. *J. Am. Chem. Soc.* **1993**, *115*, 1804.
(14) Goldberg, D. P.; Caneschi, A.; Lippard, S. J. *J. Am. Chem. Soc.* **1993**, *115*, 9299.
(15) Miller, J. S.; Epstein, A. J. *Angew. Chem., Int. Ed. Engl.* **1994**, *33*, 385.
(16) Stumpf, H. O.; Ouahab, L.; Pei, Y.; Bergerat, P.; Kahn, O. *J. Am. Chem. Soc.* **1994**, *116*, 3866.
(17) McCusker, J. K.; Christmas, C. A.; Hagen, P. M.; Chadha, R. K.; Harvey, D. F.; Hendrickson, D. N. *J. Am. Chem. Soc.* **1991**, *113*, 6114.
(18) Libby, E.; McCusker, J. K.; Schmitt, E. A.; Folting, K.; Hendrickson, D. N.; Christou, G. *Inorg. Chem.* **1991**, *30*, 3486.
(19) Christmas, C. A.; Tsai, H. L.; Pardi, L.; Kesselman, J. M.; Gantzel, P. K.; Chadha, R. K.; Gatteschi, D.; Harvey, D. F.; Hendrickson, D. N. *J. Am. Chem. Soc.* **1993**, *115*, 12483.
(20) McCusker, J. K.; Jang, H. G.; Wang, S.; Christou, G.; Hendrickson, D. N. *Inorg. Chem.* **1992**, *31*, 1874.

S0020-1669(97)01306-2 CCC: $15.00
Published on Web 04/14/1998

ferromagnets[21−25] have generated considerable optimism for the eventual realization of a new generation of magnetic materials based on molecular rather than bulk properties. From a biological perspective, the occurrence of polynuclear metal clusters at the active sites of metalloproteins demands an understanding of exchange effects for the characterization of the electronic structures of these types of proteins, as well as assessing their possible role in chemical reactivity.[26−28]

Although electron exchange is almost always thought of in the context of ground-state configurations, this is not a condition for the presence of an exchange interaction. We can enumerate three general criteria for the presence of intramolecular electron exchange: (1) each constituent involved in the exchange interaction must possess unpaired electrons; (2) there must exist some degree of spatial overlap, either directly or via the intermediacy of a bridging atom or atoms, between the magnetic orbitals on the paramagnetic sites; and (3) there must be a reasonable energetic match among all the orbitals involved in the exchange pathway. These conditions can hold true for excited states as well as ground states. Thus, the presence of exchange coupling can potentially have as profound an effect on excited-state electronic structure as it has on the ground state.

Such a change in electronic structure should influence the excited-state properties of molecules. Indeed, the basic effects of electron exchange on the static optical spectroscopy of metal complexes have been described in detail by McCarthy and Güdel.[29] Much of the detailed spectroscopic work in this area has in the past focused on doped lattices rather than discrete molecular systems; an exception to this is the extensive work that has been carried out on the exchange-coupled ligand-field states of $[Cr_3O(O_2CCH_3)_6(H_2O)_3]Cl$.[30,31] More recently, Solomon and co-workers have presented analyses in the context of their valence bond configuration interaction (VBCI) model[32,33] which reveal splittings in charge-transfer excited states arising from exchange interactions that are a factor of 10 or more greater than that found in the ground state. Other workers have reported electronic spectra of coupled molecular systems, but analyses of these spectra have been limited[34] with the notable exception of a detailed experimental and theoretical study of exchange effects on the spectroscopy of the Fe^{III}_2O core by Brown et al.[35] In terms of time-resolved spectroscopic studies, there has been virtually nothing reported in the literature on how the introduction of electron exchange manifests itself in the photoinduced *dynamics* of metal complexes;[36] this is the focus of our efforts.

This paper describes the synthesis and characterization of a transition metal−quinone dyad complex put forth as a paradigm for the study of the effect of exchange interactions on the photophysics of metal complexes. The study of transition metal−quinone complexes in general has developed over the last two decades into a rich field in terms of both their synthetic and physical chemistries.[37−39] For the purposes of our work, the advantage of using a redox-active ligand such as a quinone lies in the ability to effectively turn exchange coupling on or off in a given system (e.g., a radical semiquinone reduced to a diamagnetic catechol) without making gross changes in the overall composition of the molecule. Complexes of chromium(III) are of particular interest due to the wealth of information available concerning the photophysics of this ion in the absence of electron exchange.[40,41] Although the literature is replete with examples of compounds containing two or more quinoidal ligands bound to various metal centers, there are relatively few examples of metal−monosemiquinone/catechol complexes.[42−45] Following the lead of Benelli et al.,[46] we present here the first structurally characterized example of a chromium−monosemiquinone complex in addition to a new, high-yield, and general synthetic route into this class of compounds. We furthermore describe the magnetic and optical characteristics of these molecules, including a qualitative ligand-field analysis of their electronic structures. Finally, the role of exchange coupling on the photoinduced dynamics of these compounds is explored through the use of static and time-resolved emission and absorption spectroscopies. The results of these experiments suggest a profound effect on both radiative and nonradiative decay dynamics due to the presence of electron exchange in both the ground- and excited-state manifolds of these compounds.

Experimental Section

General. All reagents and materials from commercial sources were used as received. Solvents were purchased from either Aldrich Chemical Co. or Fisher Scientific. The ligand tris(2-aminoethyl)amine (tren) was purchased from Aldrich and vacuum distilled prior to use. $[Cr(tren)Cl_2]Cl$ was synthesized following a previously reported method.[47] All synthetic procedures involving Cr^{II} and 3,6-di-*tert*-butylcatechol were performed under an inert atmosphere using standard Schlenk techniques. Elemental analyses and mass spectra were obtained through the Analytical Facilities, University of California at Berkeley. MS measurements used standard ESMS conditions, and all spectra agreed with appropriate simulations.

3,6-Di-*tert*-butylorthobenzoquinone (3,6-DTBQ) (1). This compound was prepared by a modification of a previously reported method.[48] Toluene was added to a thick-walled Schlenk tube containing orthocatechol (2.00 g, 18.2 mmol); to this solution was added a catalytic amount of $Ti(Cat)_2$. Isobutylene (2.03 g, 36.4 mmol) was condensed into the Schlenk tube, and the reaction vessel was heated in a wax bath at 140 °C for 3 h. Following removal of solvent, the 3,6-di-*tert*-

(21) Dougherty, D. A. *Pure Appl. Chem.* **1994**, *62*, 3866.
(22) Murray, M. M.; Kaszynski, P.; Kaisaki, D. A.; Chang, W.; Dougherty, D. A. *J. Am. Chem. Soc.* **1994**, *116*, 8152.
(23) Rajca, A. *Chem. Rev.* **1994**, *94*, 871.
(24) Iwamura, H.; Koga, N. *Chem. Res.* **1993**, *26*.
(25) Inoue, K.; Iwamura, H. *J. Am. Chem. Soc.* **1994**, *116*, 3173.
(26) Bominaar, E. L.; Achim, C.; Borshch, S. A.; Girerd, J. J.; Münck, E. *Inorg. Chem.* **1997**, *36*, 3689.
(27) Girerd, J. J. *J. Chem. Phys.* **1983**, *79*, 1766.
(28) Bersuker, I. B.; Barshch, S. A. *Adv. Chem. Phys.* **1992**, *81*, 703.
(29) McCarthy, P. J.; Güdel, H. U. *Coord. Chem. Rev.* **1988**, *88*, 69.
(30) Güdel, H. U. *J. Chem. Phys.* **1985**, *82*, 2510.
(31) Schlenk, K. J.; Güdel, H. U. *Inorg. Chem.* **1982**, *21*, 2253.
(32) Tuczek, F.; Solomon, E. I. *Inorg. Chem.* **1993**, *32*, 2850.
(33) Tuczek, F.; Solomon, E. I. *J. Am. Chem. Soc.* **1994**, *116*, 6916.
(34) The spectra of a variety of oxo- and hydroxo-bridged metal dimers have been reported by several workers, but no interpretations beyond reference to the review of McCarthy and Güdel (ref 29) were generally given.
(35) Brown, C. A.; Remar, G. J.; Musselman, R. L.; Solomon, E. I. *Inorg. Chem.* **1995**, *34*, 688.
(36) Time-resolved emission spectroscopy has been used by several workers to help distinguish inequivalent sites in solid matrixes at low temperatures. See ref 29 for more details.
(37) Pierpont, C. G.; Buchanan, R. M. *Coord. Chem. Rev.* **1981**, *38*, 45.
(38) Pierpont, C. G.; Larsen, S. K.; Boone, S. R. *Pure Appl. Chem.* **1988**, *60*, 1331.
(39) Pierpont, C. G.; Lange, C. W. *Prog. Inorg. Chem.* **1994**, *41*, 331.
(40) Endicott, J. F.; Ramasami, T.; Tamilarasan, R.; Lessard, R. B.; Ryu, C. K.; Brubaker, G. R. *Coord. Chem. Rev.* **1987**, *77*, 1.
(41) Forster, L. S. *Chem. Rev.* **1990**, *90*, 331.
(42) Benelli, C.; Dei, A.; Gatteschi, D.; Pardi, L. *Inorg. Chem.* **1990**, *29*, 3409.
(43) Benelli, C.; Dei, A.; Gatteschi, D.; Pardi, L. *Inorg. Chem.* **1989**, *28*, 1476.
(44) Dei, A.; Gatteschi, D.; Pardi, L. *Inorg. Chem.* **1993**, *32*, 1389.
(45) Dei, A.; Gatteschi, D. *Inorg. Chim. Acta* **1992**, *200*, 813.
(46) Benelli, C.; Dei, A.; Gatteschi, D.; Güdel, H. U.; Pardi, L. *Inorg. Chem.* **1989**, *28*, 3089.
(47) Zipp, S. G.; Madan, S. K. *Inorg. Chem.* **1976**, *15*, 587.
(48) Belostotskaya, I. S.; Komissarova, N. L.; Dzhuaryan, E. V.; Ershov, V. V. *Isv. Akad. Nauk SSSR* **1984**, 1610.

butylorthocatechol (3,6-DTBCat) product was separated from the catalyst using a Kugelröhr. The quinone (3,6-DTBQ) was formed by addition of Ag_2O to an ether solution of the catechol and purified by elution on a silica column using a CH_2Cl_2/hexanes gradient. Evaporation of the eluent followed by sublimation yielded a green, microcrystalline product. Yield: 3.74 g (94%). ^{1}H NMR ($CDCl_3$, δ): 1.21 (s, 9 H), 6.14 (s, 1H). Anal. Calcd for $C_{14}H_{20}O_2$: C, 76.36; H, 9.09. Found: C, 76.01; H, 9.00.

[Cr(tren)(3,6-DTBCat)](PF$_6$) (2). In an inert atmosphere box, 3,6-DTBQ (0.100 g, 0.450 mmol) was reduced to 3,6-DTBCat by addition of an excess of Na metal to a solution of the quinone in 10 mL of THF. This solution was removed from the box and added using a syringe to a solution of 0.137 g (0.450 mmol) of [Cr(tren)Cl_2]Cl dissolved in 50 mL of degassed 1:1 (v/v) EtOH/H_2O. The flask was fitted with a reflux condenser, and the reaction mixture was heated at reflux for 2 days. The solution was cooled to room temperature and the volume of solvent mixture reduced using a rotary evaporator. A saturated aqueous solution of NH_4PF_6 was added, and the desired product was extracted into ethyl acetate (3 × 25 mL). The volume of the ethyl acetate solution was reduced, and the product was precipitated by addition of hexanes to yield a light green solid. This product was collected by filtration and recrystallized from CH_2Cl_2. Yield: 0.208 g (82%). Anal. Calcd for $CrC_{20}O_2N_4H_{38}PF_6$: C, 42.63; H, 6.75; N, 9.95. Found: C, 42.53; H, 6.99; N, 9.53. MS (ES): *m*/*z* 418 ([M − PF_6]$^+$, 100).

[Cr(tren)(3,6-DTBSQ)](PF$_6$)$_2$ (3). This compound can be prepared either by oxidation of **2** or via reaction of the parent quinone with Cr(tren)Cl_2.

Route A. A solution of **2** was made by dissolving 0.100 g (0.177 mmol) in 20 mL of acetonitrile. To this solution was added 0.066 g (0.26 mmol) of $AgPF_6$. Following removal of silver metal by filtration, the solution was titrated with an aqueous solution of NH_4Cl and filtered to remove the last traces of Ag^+ as AgCl. A saturated aqueous solution of NH_4PF_6 was added, and the product was extracted into ethyl acetate (3 × 50 mL). Following removal of solvent, the crude product was recrystallized by diffusion of ether into a THF solution to give yellow-green crystals. Yield: 0.093 g (74%).

Route B. This route is a modification of the method of Benelli et al.[46] $CrCl_2$ was prepared by addition of concentrated HCl (0.075 mL, 0.90 mmol) to a degassed solution of Cr metal (excess) in water. The solution was heated for 12 h to produce a light blue solution and was added to a degassed aqueous solution of tren (0.065 g, 0.45 mmol in 25 mL of H_2O), resulting in a deep blue solution. This was then added using a syringe to a degassed solution of 3,6-DTBQ (0.100 g, 0.450 mmol) in absolute ethanol. The solution was stirred for 2 h at room temperature, and the ethanol was removed by rotary evaporation. A saturated aqueous solution of NH_4PF_6 was added, and the product was extracted into ethyl acetate (3 × 40 mL). Hexanes were added to precipitate the product, leaving an impurity of Cr(3,6-DTBSQ)$_3$ in solution. The product was recrystallized by diffusion of ether into a THF solution. Yield: 0.057 g (18%). Physical data on both samples showed the compounds to be identical. $CrC_{20}O_2N_4H_{38}P_2F_{12}$: C, 33.90; H, 5.37; N, 7.91. Found: C, 33.69; H, 5.28; N, 7.79. MS (ES): *m*/*z* 564 ([M − PF_6]$^+$, 6) 209 ([M − 2PF_6]$^{2+}$, 94).

X-ray Crystallography. A single-crystal X-ray structure determination of [Cr(tren)(3,6-DTBSQ)](PF_6)$_2$ was carried out at the ChexRay facility of the Department of Chemistry, University of California at Berkeley. A dichroic (green/brown) prismatic crystal of [Cr(tren)(3,6-DTBSQ)](PF_6)$_2$ was obtained by diffusion of ether into a THF solution of the compound. One crystal having approximate dimensions of 0.30 × 0.18 × 0.14 mm was mounted on a glass fiber. Diffraction data were collected on a Siemens SMART diffractometer with graphite-monochromated Mo Kα radiation. Data were collected at −107 °C. Pertinent details regarding the structure determination are listed in Table 1, and positional parameters are given in Table 2. The unit cell parameters were obtained by a least-squares refinement using the measured positions of 6029 reflections with $I > 10\sigma$ in the range $3.00° < 2\theta < 45.00°$. Intensity data for the structure was corrected for Lorentz and polarization effects. No decay correction was applied. An empirical absorption correction based on comparison of redundant and equivalent data and an ellipsoidal model of the absorption surface was applied using the program XPREP ($T_{max} = 0.981$, $T_{min} = 0.627$).[49] The structure was solved by direct methods and expanded using Fourier techniques. All non-hydrogen atoms except for the PF_6 anions and the THF solvate were refined anisotropically while the rest were refined isotropically. Hydrogen atoms were included at calculated positions but not refined. The final cycle of least-squares refinement was based on 3006 observed reflections and 447 variable parameters, resulting in unweighted and weighted *R* factors of 0.056 and 0.070, respectively.

The anions were disordered around the F(1)−P(1)−F(2) and F(7)−P(2)−F(8) axes, respectively. The disorder in the four equatorial fluorine atoms of each anion was modeled by creating two sets of four fluorine atoms and refining on their occupancy. The major set of each was refined with anisotropic displacement parameters while the minor set remained isotropic. The relative occupancies between the major and minor sets of fluorines were 0.875/0.125 and 0.855/0.145 for P(1) and P(2), respectively.

Table 1. Crystallographic Data for [Cr(tren)(3,6-DTBSQ)](PF_6)$_2$·THF

empirical formula	$CrP_2F_{12}C_{24}N_4O_3H_{46}$
formula wt	780.57
cryst color, habit	dichroic (green/brown), prism
cryst syst	monoclinic
space group	$P2_1/c$ (No. 14)
temp (°C)	-107 ± 1
λ (Mo Kα) (Å)	0.710 69
cell dimens	
a (Å)	11.9560(2)
b (Å)	17.0715(4)
c (Å)	17.1805(4)
β (deg)	90.167(1)
V (Å^3)	3506.6(1)
Z	4
ρ (g cm^{-3})	1.482
μ (cm^{-1})	5.13
goodness of fit (*S*)[a]	1.72
R[b]	0.056
R_w[c]	0.070

[a] $S = [\sum w(|F_o| - |F_c|)^2(m - n)]^{1/2}$. [b] $R = ||F_o| - |F_c||/\sum|F_o|$. [c] $R_w = [\sum w(|F_o| - |F_c|)^2/\sum w|F_o|^2]^{1/2}$.

Table 2. Atomic Positional Parameters and Equivalent Isotropic Thermal Parameters for [Cr(tren)(3,6-DTBSQ)](PF_6)$_2$·THF

atom	*x*/*a*	*y*/*b*	*z*/*c*	B_{eq} (Å^2)
Cr(1)	0.08441(9)	0.07134(6)	0.22759(6)	2.58(2)
O(1)	0.2021(4)	0.1412(2)	0.1934(2)	2.7(1)
O(2)	0.1851(4)	−0.0052(3)	0.1886(2)	2.66(10)
N(1)	−0.0284(5)	0.1530(3)	0.2666(3)	4.0(1)
N(2)	0.1485(5)	0.0826(3)	0.3402(3)	3.4(1)
N(3)	0.0054(5)	0.0909(3)	0.1219(3)	3.0(1)
N(4)	−0.0323(4)	−0.0083(3)	0.2669(3)	2.6(1)
C(1)	0.2911(5)	0.1055(4)	0.1664(3)	2.9(1)
C(2)	0.2794(5)	0.0215(4)	0.1631(3)	2.3(1)
C(3)	0.3665(5)	−0.0278(5)	0.1316(3)	3.2(2)
C(4)	0.4601(6)	0.0121(5)	0.1122(4)	4.1(2)
C(5)	0.4733(7)	0.0951(5)	0.1179(4)	4.3(2)
C(6)	0.3912(6)	0.1445(4)	0.1429(3)	2.8(2)
C(7)	0.4007(7)	0.2341(5)	0.1442(4)	4.0(2)
C(8)	0.3140(10)	0.2687(5)	0.0901(5)	5.5(2)
C(9)	0.3823(7)	0.2640(5)	0.2279(4)	5.4(2)
C(10)	0.5154(9)	0.2603(6)	0.1189(5)	6.0(3)
C(11)	0.3486(6)	−0.1154(4)	0.1209(4)	3.4(2)
C(12)	0.4529(7)	−0.1548(5)	0.0907(4)	4.5(2)
C(13)	0.3168(7)	−0.1550(5)	0.1986(4)	4.6(2)
C(14)	0.2557(8)	−0.1281(4)	0.0626(4)	5.0(2)
C(15)	0.0293(8)	0.1980(5)	0.3291(5)	5.8(2)
C(16)	0.0982(8)	0.1517(6)	0.3781(4)	5.6(2)
C(17)	−0.0566(7)	0.2026(4)	0.1986(4)	4.6(2)
C(18)	−0.0820(8)	0.1518(5)	0.1284(4)	5.3(2)

(49) *XPREP (v 5.03) Part of the SHELXTL Crystal Structure Determination Package*, 5.03 ed.; Siemens Industrial Automation, Inc.: Madison, WI, 1995.

The THF solvate was also disordered. Three of the atoms (O(3), C(21), and C(22)) were refined with anisotropic displacement parameters while the two carbons distal from the oxygen were modeled as pairs of half-occupancy carbon atoms. The THF solvate thus appears to occupy two sites with the oxygen locked and the rest of the molecule free to "wag".

Physical Measurements. Cyclic Voltammetry. Electrochemical measurements were carried out inside an Ar-filled glovebox using a BAS 100A electrochemical analyzer. Solutions of the compounds were dissolved in distilled CH_3CN containing NBu_4PF_6 (ca. 0.1 M) as the supporting electrolyte. A standard three-electrode setup was used with a platinum working electrode, Pt wire counter electrode, and a Ag/$AgNO_3$ electrode as reference. Reported potentials versus SCE were calculated on the basis of a comparison with ferrocene measured under identical conditions.[50] On the basis of the large peak-to-peak separation obtained on the ferrocene standard ($\Delta E_p > 90$ mV), an IR compensation was applied that resulted in a more reasonable splitting of $\Delta E_p = 65$ mV for ferrocene; this same correction was applied to data collected on the chromium complexes. It should be noted that while the IR compensation brought ΔE_p values much closer to the theoretical limit of 59 mV, the values for $E_{1/2}$ were not significantly affected. No dependence of the data on scan rate over a range of 50−500 mV s^{-1} was noted.

Variable-Temperature Magnetic Susceptibility. Magnetic susceptibility data were collected using a Quantum Design MPMS SQUID magnetometer interfaced to an IBM PC. A finely ground sample of each compound was packed into a cylindrical Kel-F sample container with an inner diameter of approximately 4 mm. Data were collected in an applied field of 10.00 kG. Following each temperature change, the system was kept at the new temperature for an additional 10 min before measurements were made to ensure thermal equilibration of the sample. The data presented represent an average of three separate measurements of the sample's magnetization taken at each temperature. Data were corrected for diamagnetism using Pascal's constants[51] and reported herein as effective magnetic moments.

Static Absorption and Emission Spectra. All spectroscopic data were obtained on samples dissolved in spectral- or HPLC-grade solvents. Electronic absorption spectra were recorded using a Perkin-Elmer Lambda 9 dual-beam spectrometer. Spectra were collected with a resolution of 0.23 nm at a scan rate of 250 nm/min.

Emission spectra were collected using an Instruments SA/Jobin Yvon-Spex Fluoromax photon-counting fluorimeter equipped with a Xe arc lamp excitation source and a Hamamatsu R928P photomultiplier tube operating at −900 V dc. Data were obtained on thoroughly deoxygenated solutions of each complex having an optical density of ca. 0.1 (1 cm path length) at the excitation wavelength. Background measurements on the solvent blanks revealed no signals other than the expected Raman lines of the neat solvent. The resolution of each spectrum is estimated to be ±2 nm on the basis of the RLD of the emission monochromator and the slit setting of the instrument. Spectra were corrected for instrument response using a NIST standard of spectral irradiance (Optronic Laboratories, Inc., OL220M tungsten quartz lamp). All subsequent data manipulations were carried out using the corrected spectra. In converting wavelength to energy units, the correction of Parker and Rees was applied.[52] Low-temperature data were collected using a Janis SVT-100 optical cryostat. Temperature control was achieved using heating filaments and two matched diodes placed approximately equidistant above and below the sample region. The heaters and the diodes were coupled to two LakeShore model 321 automated temperature control units. Temperature stability was better than ±0.2 K; the absolute accuracy is estimated to be on the order of ±1 K.

Time-Resolved Emission and Absorption Spectroscopy. Time-resolved emission and absorption data were collected using a Nd:YAG/optical parametric oscillator-based nanosecond laser spectrometer, the details of which are described elsewhere.[53]

Results and Discussion

Synthesis of Cr−Quinone Dyads. The desirability of having a chemical system consisting of only two interacting paramagnetic components for the initial study of exchange effects on photoinduced dynamics led us to the idea of a metal−quinone dyad. The nature of the counterligand(s) was relatively unimportant, provided that they could not engage in exchange interactions or, ideally, in redox chemistry. A thorough search of the literature yielded only two examples of this motif for chromium(III). Benelli et al.[46] reported the synthesis and partial characterization of $[Cr(CTH)(3,5\text{-DTBSQ})]_2(PF_6)_3Cl$ and $[Cr(CTH)(TCCat)](PF_6)$, where 3,5-DTBSQ is 3,5-di-*tert*-butylorthosemiquinone, TCCat is 3,4,5,6-tetrachloroorthocatechol, and CTH is 5,7,7,12,14,14-hexamethyl-1,4,8,11-tetraazacyclodecane, a tetradentate macrocycle. This system seemed to be a reasonable starting point for our research, and we were able to reproduce the results reported by these authors (**Route B**). Their synthetic route involves a redox reaction between a Cr^{II} starting material ($Cr(CTH)Cl_2$) and the parent quinone. The approach is similar to that used for forming tris-semiquinone complexes, e.g., Cr^0 plus 3 equiv of quinone to yield a $Cr(SQ)_3$ complex.[54,55] An advantage of this synthetic strategy is the lability of the Cr^{II} synthon toward loss of the chloride ligands. However, chromatographic work revealed that in our hands several other products are also formed in this reaction. One that was positively identified was $Cr(3,6\text{-DTBSQ})_3$, identified on the basis of a comparison with an authentic sample. This result, in addition to the fact that both semiquinone and catechol complexes are obtained by Benelli et al. from the same general scheme, is illustrative of the complex redox chemistry that is occurring in this reaction.

We therefore developed an alternative route into this class of molecules (**Route A**). Due to the possibility of dimer formation in the case of the 3,5-di-*tert*-butylorthoquinone,[39,56] we have focused on compounds of the 3,6 isomer in which sterics prevent the oxygen donors of the quinoid from bridging between two metal centers. The counterligand tren was selected for the prototype due to the fact that it forms a single isomer when bound to a metal, as opposed to CTH which can exist in both meso and racemic forms. The synthesis of $[Cr(tren)(3,6\text{-DTBCat})]^+$ (and, subsequently, $[Cr(tren)(3,6\text{-DTBSQ})]^{2+}$) proceeds cleanly and in high yield from the Cr^{III} starting material with little formation of side products. The well-known inertness of Cr^{III} toward substitution necessitates a longer reaction time than the Cr^{II} route, but the improvement in overall yield testifies to the cleanliness of the reaction despite the added reflux time. The reaction to make the catechol complex must be carried out in an inert atmosphere, as the sodium salt of the catechol ligand readily oxidizes to the quinone upon dissolution in the presence of oxygen. Once bound to the metal, the catechol complex is much more stable with respect to oxidation and can be kept as a solid for long periods of time without evidence of decomposition. Solutions of the catecholate complex are also reasonably stable, although they will oxidize to the semiquinone form after several hours in air. The semiquinone complex is very stable

(50) Barrett, W. C.; Johnson, H. W.; Sawyer, D. T. *Anal. Chem.* **1984**, *56*, 1890.
(51) *Theory and Applications of Molecular Paramagnetism*; Boudreaux, E. A., Mulay, L. N., Eds.; John Wiley and Sons: New York, 1976.
(52) Parker, C. A.; Rees, W. T. *Analyst (London)* **1960**, *85*, 587.
(53) Damrauer, N. H.; Boussie, T. R.; Devenney, M.; McCusker, J. K. *J. Am. Chem. Soc.* **1997**, *119*, 8253.
(54) Pierpont, C. G.; Downs, H. H.; Rukavina, T. G. *J. Am. Chem. Soc.* **1974**, *96*, 5573.
(55) Vleck, A. J. *Inorg. Chem.* **1986**, *25*, 522.
(56) Buchanan, R. M.; Fitzgerald, B. J.; Pierpont, C. G. *Inorg. Chem.* **1979**, *18*, 9.

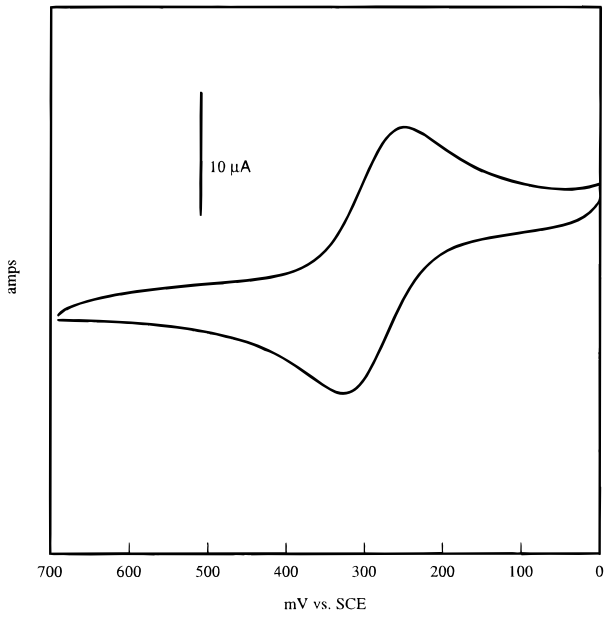

Figure 1. Cyclic voltammogram of [Cr(tren)(3,6-DTBSQ)]$(PF_6)_2$ in degassed acetonitrile.

in both solution and the solid state, with no evidence of decomposition in either case upon long-term exposure to air.

It should be pointed out that, although we will focus only on the tren/3,6-di-*tert*-butylorthoquinone-based complexes in this report, our synthetic strategy provides a very general entry into this class of compounds: we have shown it to work for several different parent quinones (e.g., 3,6-DTBQ, 3,5-DTBQ, and TCQ) as well as a range of σ-donor (e.g., tren, trien, CTH, ethylenediamine) and π-donor/π-acceptor ligands (e.g., 2,2′-bipyridine).[57] We have also tried the approach of Benelli et al. using these other ligands and have found that the redox route works almost as well as the Cr^{III} reaction for all of these other systems with the exception of CTH. At present, the reason for our difficulties with reactions involving the CTH counterligand are not clear.

Electrochemistry. The clean, one-electron redox chemistry implied by the success of **Route A** is evident in the electrochemistry exhibited by these dyads. In Figure 1 is shown a cyclic voltammogram of [Cr(tren)(3,6-DTBSQ)]$(PF_6)_2$ in degassed CH_3CN. The one-electron wave at +0.288 V (vs SCE) is analytically reversible with a peak-to-peak separation of 59 mV, while an irreversible wave is observed at +1.1 V (not shown). We assign both of these processes as being associated with the quinoidal ligand. These assignments are based both on the chemically reversible redox behavior suggested by **Route A** and on the similarity of our data to those obtained for related monoquinone complexes such as $[Co(trien)(3,5\text{-DTBCat})]^+$ [58] and $[Cr(CTH)(3,5\text{-DTBCat})]^+$,[46] as well as tris complexes such as $Cr(3,5\text{-DTBSQ})_3$.[59,60] The reversible wave at 0.288 V is therefore ascribed to cycling between the semiquinone and catechol forms of the compound (eq 1a), while the irreversible oxidation at +1.1 V is assigned as an oxidation from semiquinone to quinone (eq 1b). The irreversibility of this process

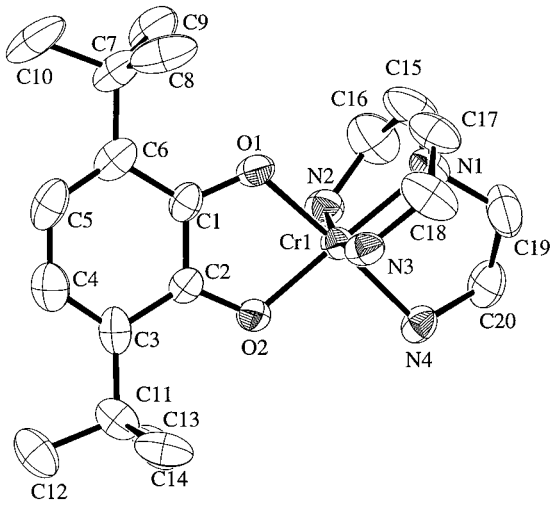

Figure 2. Drawing of the cation of [Cr(tren)(3,6-DTBSQ)]$(PF_6)_2$ from a single-crystal X-ray structure determination. See Table 1 for crystallographic details and Tables 3 and 4 for structural details.

$$[Cr(tren)(3,6\text{-DTBSQ})]^{2+} \underset{-e^-}{\overset{+e^-}{\rightleftharpoons}} [Cr(tren)(3,6\text{-DTBCat})]^{+} \quad (1a)$$

$$E_{1/2} = +0.288 \text{ V}$$

$$[Cr(tren)(3,6\text{-DTBSQ})]^{2+} \xrightarrow{-e^-} [Cr(tren)(3,6\text{-DTBQ})]^{3+} \quad (1b)$$

$$E_{ox} = +1.1 \text{ V}$$

is not surprising due to the fact that the fully oxidized quinone is a very poor ligand. Formation of this species following oxidation of the semiquinone complex will likely result in ligand loss, hence an irreversible wave in the cyclic voltammogram.

Reductive scans out to −2.0 V failed to show any signal attributable to the Cr^{III}/Cr^{II} couple. Again, this is consistent with what has been observed in other Cr-catecholate complexes[61] and testifies to the stability of the oxidation state of the metal when bound to the quinoidal ligand.

X-ray Structure of [Cr(tren)(3,6-DTBSQ)](PF$_6$)$_2$. [Cr(tren)(3,6-DTBSQ)]$(PF_6)_2$ crystallizes as a THF solvate in the monoclinic space group $P2_1/c$. Crystallographic details are given in Table 1, with positional parameters and selected bond distances and angles given in Tables 2, 3, and 4, respectively. An ORTEP drawing of the cation is shown in Figure 2. It can be seen that, as expected, the molecule has a relatively simple structure. The environment about the metal ion is a distorted octahedron with four aliphatic nitrogens from the tren and two oxygen donors from the orthosemiquinone. Bond angles in the coordination sphere deviate slightly from the expected 90° and 180°, due mainly to the reduced bite angle of the tetradentate ligand in spanning all four coordination sites. The Cr−N bond distances are unremarkable with an average of 2.075 ± 0.015 Å, similar to those observed for related complexes such as $[Cr(en)_3]^{3+}$.[62] The Cr−O distances are somewhat more dissimilar to each other at 1.937(4) Å (Cr(1)−O(1)) and 1.901(4) Å (Cr(2)−O(2)). However, the overall symmetry of the ligand field can be approximated quite reasonably as C_{2v}.

The geometric details associated with the semiquinone are the most interesting aspect of the structure. It has been found that, for orthoquinone-type ligands bound to first-row metals,

(57) Wheeler, D. E.; McCusker, J. K. Unpublished results.
(58) Wicklund, P. A.; Brown, D. G. *Inorg. Chem.* **1976**, *15*, 396.
(59) Sofen, S. R.; Ware, D. C.; Cooper, S. R.; Raymond, K. N. *Inorg. Chem.* **1979**, *18*, 234.
(60) Buchanan, R. M.; Pierpont, C. G. *J. Am. Chem. Soc.* **1980**, *102*, 4951.
(61) Other monosemiquinone metal systems such as [Co(trien)(3,5-DTBSQ)]$^{2+}$ show electrochemical behavior associated with oxidation of the ligand.
(62) Whuler, A.; Brouty, C.; Spinat, P.; Herpin, P. *Acta Crystallogr., Sect. B* **1977**, *33*, 2877.

Table 3. Selected Bond Lengths (Å) for [Cr(tren)(3,6-DTBSQ)]-$(PF_6)_2$·THF

Cr(1)−O(1)	1.937(4)	Cr(1)−O(2)	1.901(4)
Cr(1)−N(1)	2.055(6)	Cr(1)−N(2)	2.089(5)
Cr(1)−N(3)	2.072(5)	Cr(1)−N(4)	2.064(5)
O(1)−C(1)	1.312(8)	O(2)−C(2)	1.293(7)
N(1)−C(15)	1.487(9)	N(1)−C(17)	1.482(9)
N(1)−C(19)	1.52(1)	N(2)−C(16)	1.476(10)
N(3)−C(18)	1.478(9)	N(4)−C(20)	1.483(9)
C(1)−C(2)	1.442(10)	C(1)−C(6)	1.429(9)
C(2)−C(3)	1.445(9)	C(3)−C(4)	1.353(10)
C(3)−C(11)	1.52(1)	C(4)−C(5)	1.43(1)
C(5)−C(6)	1.36(1)	C(6)−C(7)	1.53(1)
C(7)−C(8)	1.51(1)	C(7)−C(9)	1.541(9)
C(7)−C(10)	1.51(1)	C(11)−C(12)	1.51(1)
C(11)−C(13)	1.545(10)	C(11)−C(14)	1.51(1)
C(15)−C(16)	1.42(1)	C(17)−C(18)	1.52(1)
C(19)−C(20)	1.53(1)		

Table 4. Selected Bond Angles (deg) for [Cr(tren)(3,6-DTBSQ)]-$(PF_6)_2$·THF

O(1)−Cr(1)−O(2)	81.6(2)	O(1)−Cr(1)−N(1)	99.2(2)
O(1)−Cr(1)−N(2)	87.7(2)	O(1)−Cr(1)−N(3)	88.0(2)
O(1)−Cr(1)−N(4)	175.9(2)	O(2)−Cr(1)−N(1)	177.9(2)
O(2)−Cr(1)−N(2)	99.1(2)	O(2)−Cr(1)−N(3)	95.1(2)
O(2)−Cr(1)−N(4)	95.3(2)	N(1)−Cr(1)−N(2)	82.8(2)
N(1)−Cr(1)−N(3)	83.0(2)	N(1)−Cr(1)−N(4)	84.0(2)
N(2)−Cr(1)−N(3)	164.3(2)	N(2)−Cr(1)−N(4)	90.2(2)
N(3)−Cr(1)−N(4)	95.0(2)		

the bond lengths within the ring of the quinone provide a strong indication as to the oxidation state of the ligand.[39] Specifically, if the quinone exists in the catecholate form, all of the C−C bond distances should be nearly identical due to the aromatic nature of that species. The semiquinone form, however, should exhibit alternating short and long C−C bonds because of the more localized nature of the double bonds within the ring. Given this, we find that the intraligand bond distances in [Cr(tren)-(3,6-DTBSQ)]$^{2+}$ are clearly consistent with a semiquinone formulation: C(3)−C(4) and C(5)−C(6) are found to be 1.353-(10) and 1.36(1) Å, respectively, whereas C(1)−C(2), C(2)−C(3), C(4)−C(5), and C(1)−C(6) are all approximately 1.435 ± 0.010 Å. Secondary structural confirmation of the intermediate reduction level of the ligand comes from the C−O bond distances: C(1)−O(1) and C(2)−O(2) distances of 1.312(8) and 1.293(7) Å are much shorter than the 1.35 Å expected of a catechol[59] and in the range of that found for other first-row metal semiquinone complexes.[37,39,59,60] The shorter C(2)−O(2) distance relative to C(1)−O(1) suggests more double-bond character in the C(2)−O(2) bond.

Chart 1

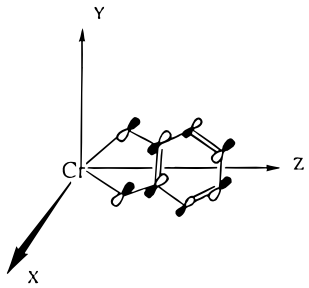

A stereoview of the packing diagram for [Cr(tren)(3,6-DTBSQ)]$(PF_6)_2$ (minus the anions and the THF solvate) is shown in Figure 3. From this figure, it can be seen that all of the cations line up with the intramolecular *z*-axis (see Chart 1) parallel to the *a*-axis of the unit cell. We believe this fortuitous alignment gives rise to the dichroism observed for these crystals and is a direct consequence of the exchange coupling present in the molecule (vide infra).

Ground-State Characterization: Magnetic Susceptibility. The effect of electron exchange within the ground-state configuration of this class of molecules can be probed by variable-temperature magnetic susceptibility measurements. Electron exchange in these low-symmetry complexes can be described

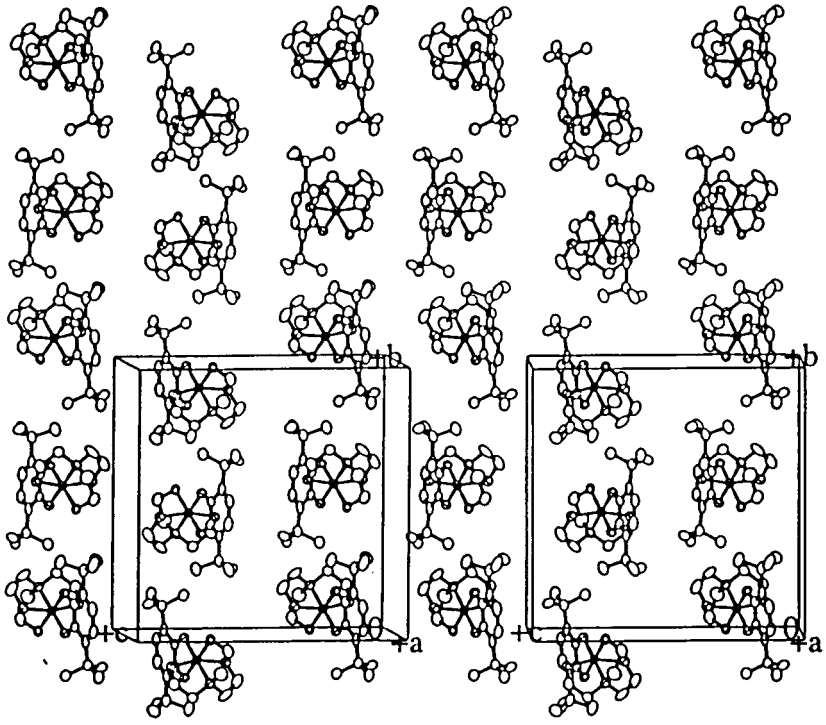

Figure 3. Stereoview of the packing diagram of [Cr(tren)(3,6-DTBSQ)]$(PF_6)_2$. The PF_6 anions and THF solvate have been omitted for clarity.

using a simple Heisenberg exchange Hamiltonian of the form in eq 2,

$$H = -2J_{ij}\mathbf{S}_i\cdot\mathbf{S}_j \qquad (2)$$

where $\mathbf{S}_i$ and $\mathbf{S}_j$ are spin operators on the ith and jth spin centers (e.g., the Cr^{III} ion and the semiquinone radical) and J_{ij} is the electron exchange integral that gauges the magnitude of the electronic coupling between the spin centers.

Plots of the effective magnetic moment versus temperature in the range 5−350 K for solid samples of [Cr(tren)(3,6-DTBCat)](PF_6) and [Cr(tren)(3,6-DTBSQ)]$(PF_6)_2$ are given in Figure 4. The value of $\mu_{eff} = 3.85 \pm 0.1\ \mu_B$ for [Cr(tren)(3,6-DTBCat)](PF_6) is in excellent agreement with the spin-only value of 3.87 μ_B expected for an $S = {}^3/_2$ ion and is consistent with the Cr^{III}−catechol formulation of the compound. The slight positive slope observed in the data with increasing temperature is likely due to temperature-independent paramagnetism (TIP).[63] The effective moment data for [Cr(tren)(3,6-DTBSQ)]$(PF_6)_2$ also exhibit temperature-independent behavior. However, the value of $\mu_{eff} = 2.85 \pm 0.1\ \mu_B$ is characteristic of a $S = 1$ state ($\mu_{spin-only} = 2.83\ \mu_B$) and indicates the presence of a strong antiferromagnetic interaction between the unpaired electrons on the Cr^{III} ($S = {}^3/_2$) and the semiquinone ligand ($S = {}^1/_2$). In fact, the interaction is so strong that there is no evidence for any thermal population of the excited $S = 2$ state in this compound even at 350 K; these results are similar to those reported by Benelli et al. for the room-temperature effective moment of [Cr(CTH)-(3,5-DTBSQ)]$_2(PF_6)_3Cl$.[46] Such a lack of temperature dependence in the effective magnetic moment precludes us from quantifying the magnitude of the exchange coupling in this complex. However, assuming that we could detect a population of ca. 7% of the $S = 2$ state at 350 K,[64] we can place a very conservative lower limit of $-350\ cm^{-1}$ on the value of J based on eq 2.

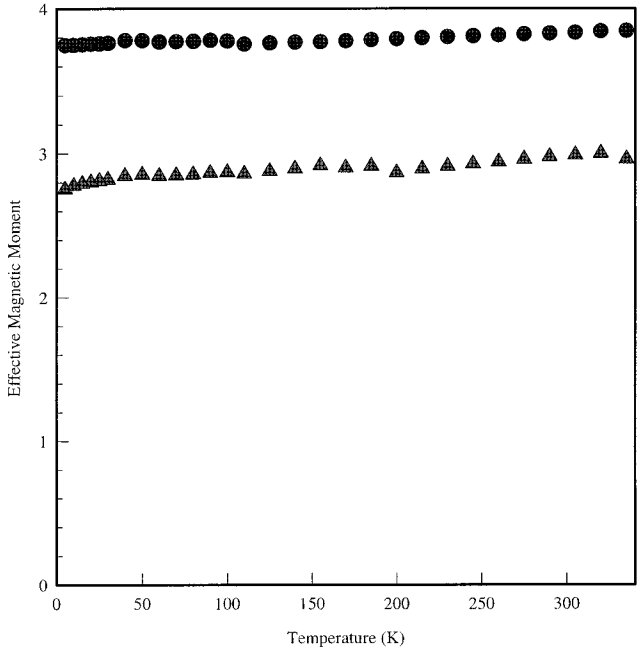

Figure 4. Plot of effective magnetic moment versus temperature for [Cr(tren)(3,6-DTBCat)](PF_6) (circles) and [Cr(tren)(3,6-DTBSQ)]$(PF_6)_2$ (triangles).

One issue that should be addressed is whether the electronic structure of this compound should be thought of in terms of an exchange-coupled Cr^{III}−semiquinone dyad, or in terms of molecular orbitals formed due to significant, direct overlap between magnetic orbitals on the metal and the ligand. We believe that, despite the indeterminately large magnitude of the exchange integral in this complex, it is still appropriate to think of the constituents of these dyads in terms of a coupling of two spin centers having distinct oxidation states. Our reasoning for this arises from several considerations. First, although temperature dependence is not observed in these dyads, Cr(3,6-DTBSQ)$_3$ exhibits a pronounced temperature dependence in its effective magnetic moment that can be easily modeled by a spin Hamiltonian of the form given in eq 2.[57] Second, the fact that the reduction potential of the semiquinone ligand in this Cr^{III} complex is very similar to that found for [Co(trien)(3,5-DTBSQ)]$^{2+}$, a compound containing a diamagnetic metal center, suggests that the nature of the LUMOs in the two complexes are comparable and, more importantly, are likely to be ligand-based. Third, as will be described below, certain features in the optical spectrum of this compound are characteristic of ligand-field transitions of Cr^{III}. Such electronic states would be essentially nonexistent if the Cr^{III} ion were involved in a highly covalent interaction with the semiquinone ligand. Finally, we have recently completed a density functional theory analysis of the ground-state electronic structure of [Cr(tren)-(3,6-DTBSQ)]$^{2+}$ which further supports a Heisenberg spin-coupled description. These results are described in detail elsewhere.[65]

Electronic Absorption Spectra. We can begin to gain insight into how exchange coupling is affecting the excited-state manifold of the Cr^{III}−semiquinone complex by comparing and contrasting the electronic absorption spectra of the semiquinone and catechol species. An overlay of the absorption spectra of [Cr(tren)(3,6-DTBCat)](PF_6) and [Cr(tren)-(3,6-DTBSQ)]$(PF_6)_2$ in 4:1 EtOH/MeOH at room temperature is illustrated in Figure 5. To interpret these spectra, we have defined our C_{2v} coordinate system as indicated in Chart 1. It should be noted that this coordinate system, dictated by the location of the C_2 axis through the C(1)−C(2) bond (as opposed to along a bond axis), corresponds to a $\pi/4$ rotation of the coordinate system typically used for deriving the O_h correlation tables. We have therefore rederived the $O_h \rightarrow C_{2v}$ correlation for the relevant basis sets and term states of the d^3 configuration based on our coordinate system; these are listed in Tables 5 and 6, respectively.

Assignment of the visible portion of the spectrum of [Cr-(tren)(3,6-DTBCat)]$^+$ is straightforward. The broad absorption centered at 600 nm ($\epsilon_{\lambda=600nm} = 80\ M^{-1}\ cm^{-1}$) can be attributed to the spin-allowed ($^4A_2$, $^4B_1$, $^4B_2$) ← $^4A_1$ transition ($^4T_{2g}$ ← $^4A_{2g}$ parentage). A second, higher energy spin-allowed transition is commonly observed in the ligand-field spectra of Cr^{III}. However, this absorption, derived from the octahedral $^4T_{1g}$ ← $^4A_{2g}$ transition, is largely obscured in [Cr(tren)(3,6-DTBCat)]$^+$ save for a very weak shoulder near 450 nm due to the broad, more intense band centered near 380 nm that tails out into the visible. Finally, no feature assignable to the ($^2A_1$, $^2A_1$) ← $^4A_1$ intraconfigurational transition is observed in the red, consistent with the small value of ϵ expected for this spin-forbidden band.

Several absorptions are present in the ultraviolet: one (or two) at ca. 340 nm, and a third much higher in energy (not

(63) TIP, although providing a constant, temperature-independent offset in the molar susceptibility, will manifest itself as a $T^{1/2}$ dependence of μ_{eff}.

(64) A 7% population of $S = 2$ at 350 K would give a moment of 3.00 μ_B, a difference well within the detection limits of our experiment.

(65) Rodriguez, J. H., Wheeler, D. E., McCusker, J. K. Submitted for publication.

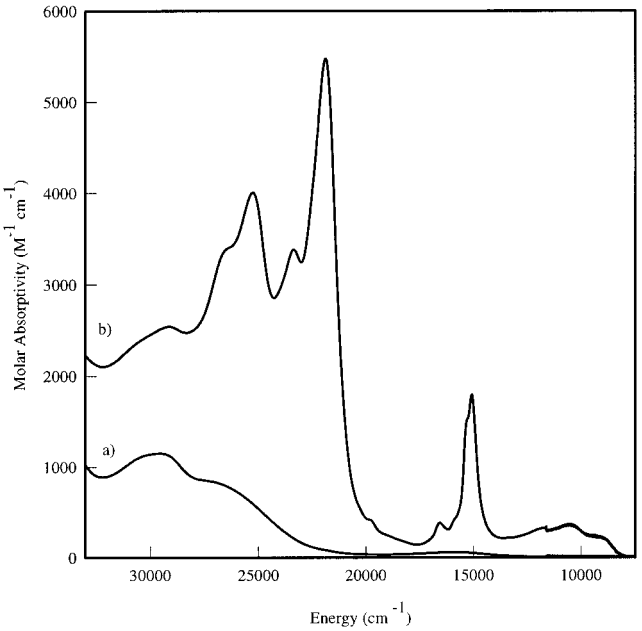

Figure 5. Room-temperature absorption spectra of (a) [Cr(tren)(3,6-DTBCat)](PF_6) and (b) [Cr(tren)(3,6-DTBSQ)](PF_6)$_2$ in 4:1 EtOH/MeOH. The discontinuity near 12 000 cm^{-1} is an instrumental artifact due to a detector change in the spectrometer.

Table 5. Basis Set Transformations in C_{2v} Symmetry for the Axis System in Chart 1

Cartesian axes	ligand orbitals
$\Gamma_x \rightarrow b_1$	$\Gamma_{HOMO} \rightarrow b_1$
$\Gamma_y \rightarrow b_2$	
$\Gamma_z \rightarrow a_1$	

Cr d-orbitals
$\Gamma_{xy} \rightarrow a_2$
$\Gamma_{xz} \rightarrow b_1$
$\Gamma_{yz} \rightarrow b_2$
$\Gamma_{z^2} \rightarrow a_1$
$\Gamma_{x^2-y^2} \rightarrow a_1$

Table 6. Correlation Table from O_h to C_{2v} Symmetry for the Axis System in Chart 1

O_h		C_{2v}
A_{2g}	→	A_1
E_g	→	$A_1 + A_1$
T_{1g}	→	$A_2 + B_1 + B_2$
T_{2g}	→	$A_2 + B_1 + B_2$

shown). The failure to observe either the Cr^{III}/Cr^{II} or Cr^{III}/Cr^{IV} couples in the electrochemistry of this compound suggests that charge-transfer bands (LMCT or MLCT) would likely be found in the ultraviolet region of the spectrum. Thus, the transitions blue of 400 nm might be due to spin-allowed CT bands, or ligand-centered ($n \rightarrow \pi^*$ or $\pi \rightarrow \pi^*$) transitions of the catechol. Unfortunately, distinguishing between these possibilities a priori is difficult. We therefore carried out a variable solvent study to look for solvatochromic shifts in the absorption features. The causes underlying solvatochromism are well-known. Charge-transfer bands are particularly susceptible to solvatochromic effects due to the highly polar nature of the Franck−Condon state. Spectra collected in THF, DMSO, and CH_3CN, as well as the 4:1 EtOH/MeOH data, are shown in Figure 6. It can be seen that none of the principal absorption features exhibit any significant solvatochromic shift across this solvent series. This is to be expected for the ligand-field absorptions in the visible, but we were surprised not to observe a solvent effect on any of

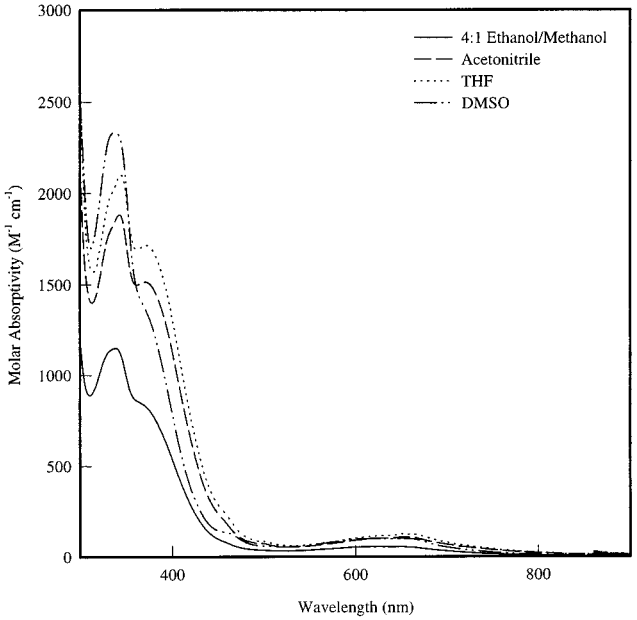

Figure 6. Room-temperature absorption spectra of [Cr(tren)(3,6-DTCat)](PF_6) in various solvents.

the ultraviolet absorptions. LMCT bands in related Fe^{III}−semiquinone complexes, for example, exhibit pronounced solvatochromism, undergoing a blue shift in polar relative to nonpolar solvents.[44] On the basis of this comparison, our observations provide a compelling argument for assigning all of the ultraviolet transitions as intraligand in nature. However, it is not *always* the case that charge-transfer bands are solvatochromic,[66] so caution must be exercised in dismissing assignment of a band as charge-transfer solely on the basis of this type of negative result.

The data in Figure 6 reveal changes in the molar extinction coefficient of all of the ultraviolet bands with changes in solvent, although no obvious trends with solvent dielectric,[67] dipole moment, etc. are apparent. There are no significant changes in the spectral bandwidth of these absorptions across the solvent series, suggesting that the changes in molar extinction are reflective of true variations in the oscillator strengths of the absorptions. This observation is seemingly at odds with the lack of solvatochromism. If the magnitudes of the transition dipoles are indeed strongly coupled to the solvent, it is not clear to us why the molar extinction coefficient of the transitions would change with solvent but not their energies. Further studies of the spectroscopy of this compound are currently underway.

The absorption spectrum of [Cr(tren)(3,6-DTBSQ)](PF_6)$_2$ is considerably more complex than that of its catecholate analogue. In fact, to our knowledge no other metal−semiquinone complex shows as rich an absorption spectrum as is seen for Cr^{III}. For the present, we will forego any discussion of the features in the ultraviolet due to their already ambiguous nature in the absence of electron exchange. One can identify three other principal regions in the spectrum of the semiquinone complex: (1) the red-green region, characterized by a pair of sharp, closely spaced, and moderately intense absorptions around 665 nm, as

(66) Lever, A. B. P. *Inorganic Electronic Spectroscopy*, 2nd ed.; Elsevier: New York, 1984.

(67) The dielectric constant quoted in common references for a given solvent is usually the bulk, continuum dielectric. This may or may not be an accurate reflection of the effective dielectric of the first solvation shell about a given chromophore.

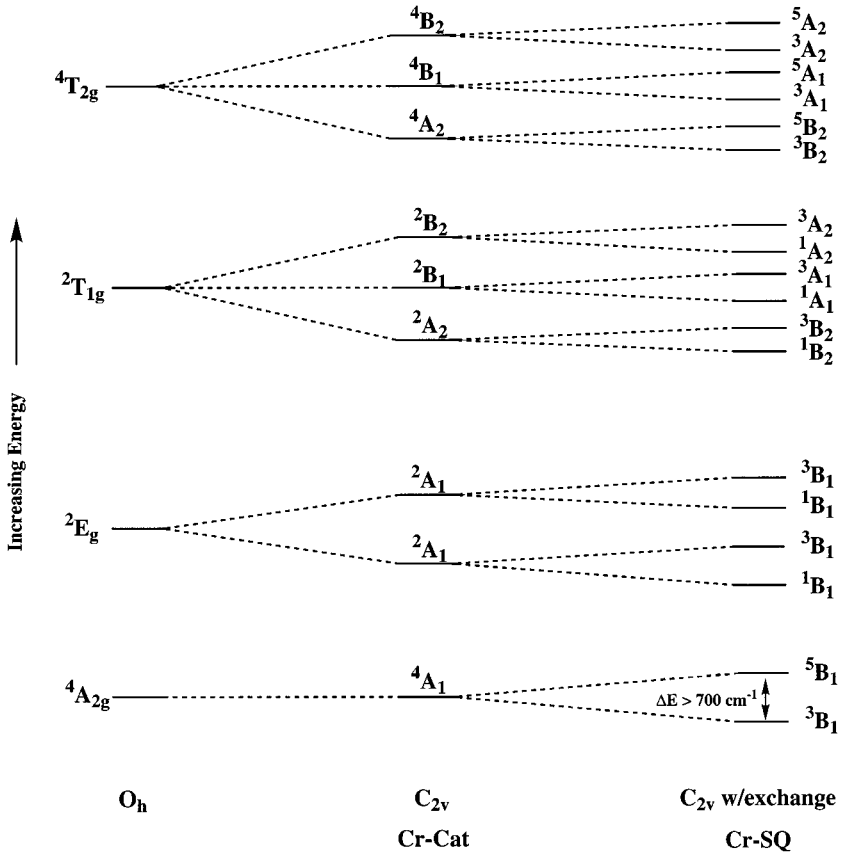

Figure 7. Results of a ligand-field theory analysis of a Cr^{III}−quinone dyad. The first column indicates several of the lowest-lying ligand-field states present in a d^3 metal ion in O_h symmetry. The second column represents the splitting upon lowering the symmetry to C_{2v} and is appropriate for $[Cr(tren)(3,6\text{-DTBCat})]^+$ in the coordinate system depicted in Chart 1. The third column represents splitting in C_{2v} when the unpaired spins of the metal couple to a $S = {}^1/_2$ spin of b_1 symmetry (i.e., $[Cr(tren)(3,6\text{-DTBSQ})]^{2+}$). The relative ordering of the spin-coupled states for the Cr−SQ diagram assumes antiferromagnetic coupling in the excited states; the ordering of the orbital terms is arbitrary. Other states that are present such as the $^4T_{1g}$ and $^2T_{2g}$ have been omitted for clarity, but may also be contributing to the absorption spectrum.

well several weaker, sharp features between 500 and 650 nm; (2) the near IR, consisting of three bands centered near 950 nm; and (3) the blue region, consisting of several rather intense features in the range 400−475 nm. We shall discuss each of these regions in turn.

Region 1. Our principal focus is on region 1, where the most pronounced feature is the pair of absorptions centered at ca. 665 nm. These bands occur in the same wavelength range that one would expect for the spin-forbidden intraconfigurational ($^2A_1$, $^2A_1$) ← $^4A_1$ transition.[68] The narrow bandwidth of ca. 200 cm^{-1} for each of the two bands[69] suggests transitions between nested potential surfaces, but the oscillator strengths are 3−4 orders of magnitude more intense than that expected for a spin-forbidden ligand-field transition. Similar features were observed by Benelli et al.[46] in the spectra of both $[Cr(CTH)(3,5\text{-DTBSQ})]^{2+}$ and $[Cr(CTH)(TCSQ)]^{2+}$. In fact, this transition seems to be characteristic of the Cr^{III}−SQ dyad motif: all of the other complexes of this type that we have prepared exhibit this same spectroscopic tag.

A group theoretical analysis of the electronic structure of this class of molecules including the effects of electron exchange provides a reasonable qualitative explanation of this feature. As indicated in Table 5, the HOMO of the semiquinone ligand illustrated in Chart 1 has b_1 symmetry in C_{2v}; the ground term state for the ligand is therefore $^2B_1$. The symmetry effects of electron exchange can be determined via a direct product analysis of the coupled terms, i.e., the $^2B_1$ of the semiquinone and the various term states of the Cr^{III} ion. This is illustrated in Figure 7, along with the term states of the Cr^{III}−catechol complex in C_{2v} symmetry and their parent terms in O_h. The spin states indicated for the Cr^{III}−SQ dyad reflect the two possible vectorial combinations of the $S = {}^1/_2$ semiquinone radical with the spin of the Cr^{III} term to which it is coupled. On the basis of the magnetic data presented in Figure 4, the ground state of $[Cr(tren)(3,6\text{-DTBSQ})]^{2+}$ is $^3B_1$, with the $^5B_1$ state lying >700 cm^{-1} higher in energy. This diagram, although qualitative, serves to underscore the enormous change in electronic structure that accompanies the introduction of electron exchange into both the ground- and excited-state configurations of the molecule.

While the intraconfigurational transition(s) are formally spin-forbidden in the catecholate complex, they are replaced by two spin-allowed $^3B_1$ ← $^3B_1$ absorptions in the exchange-coupled semiquinone complex. We assign the two bands near 665 nm in $[Cr(tren)(3,6\text{-DTBSQ})]^{2+}$ as these two $^3B_1$ ← $^3B_1$ transitions on the basis of several factors. First, the intraconfigurational nature of the transition remains largely unchanged under the influence of spin exchange. With the exception of the spin-symmetry allowedness of the transition, many of the characteristic features of the transition (e.g., spectral bandwidth) should not be significantly affected. Second, the weak dependence of

(68) The energy of the parent ^2E_g state is relatively insensitive to ligand-field strength. Thus, the ^2E_g ← $^4A_{2g}$ transition is usually observed within a narrow range of wavelengths for most Cr^{III} complexes.

(69) This band was fitted to two Gaussians using Peakfit (4.01 ed.; Jandel Scientific Software, Inc., 1995) in order to estimate the magnitude of the splitting between the two transitions.

the $^2A_1$ term state energy on ligand-field strength suggests that the absorption maximum for the semiquinone complex will be close to what would be observed in the catecholate species. Given this, the 725 nm emission maximum of the catecholate (vide infra) infers a Stokes shift very typical of ^{2}E-based emission often observed in complexes of Cr^{III}.[41] A third point is the observed dichroism of single crystals of the compound. As the packing diagram in Figure 3 illustrates, all of the cations in the unit cell align with their molecular C_2 axes parallel to the *a*-axis of the crystal. The $^3B_1 \leftarrow {}^3B_1$ transition is *z*-polarized. Thus, looking down the appropriate axis of the crystal the compound should appear green (i.e., both the blue and red absorptions will be present), whereas viewing along either of the other two axes should cause the 665 nm bands to extinguish and impart an orange-brown color to the crystal. The polarization characteristics of these bands are currently being quantified by single-crystal polarized absorption spectroscopy and will be described in a separate report.[70] Finally, on the basis of Figure 7, the small splitting between these bands of ca. 150 cm^{-1} corresponds in our present model to the low-symmetry ligand-field (LSLF) distortion that ostensibly lifts the degeneracy of the ^2E_g term upon reduction from O_h to C_{2v}. The magnitude of the LSLF splitting seen in this compound is similar to what has been previously reported for other low-symmetry Cr^{III} complexes[41] and is qualitatively consistent with the degree of ligand-field disparity between the nitrogen- and oxygen-based donors about the metal core.

A $^3B_1 \leftarrow {}^3B_1$ transition has an expected extinction coefficient of ca. 10^2 M^{-1} cm^{-1}. This assignment therefore accounts for several orders of magnitude in increased intensity relative to a $^2A_1 \leftarrow {}^4A_1$ transition, but still leaves a disparity of approximately an order of magnitude in the experimental spectrum. We agree with the assessment of Benelli et al. that the ligand-field bands in these complexes likely have significant charge-transfer character due to admixture with nearby CT state(s). Some degree of mixture between charge-transfer and ligand-field states in the electronic manifolds of these complexes is reasonable to expect given the magnitude of the electron exchange interaction present. Whether the charge-transfer state or states involved in the intensity stealing correspond to the intense band at 460 nm will be discussed below. However, we emphasize that inclusion of exchange effects accounts for ca. 75% of the experimentally observed increase in intensity for this transition and is therefore the major factor contributing to this spectral feature.

Several other weaker, sharp features are observed to the high-energy side of the 665 nm set. On the basis of their spectral positions and bandwidths, we tentatively ascribe these bands to formerly spin-forbidden transitions derived from the $^2T_{1g}$ octahedral term. However, this assignment will also be re-examined in the singal-crystal work alluded to above.

Region 2. The near-infrared portion of the spectrum exhibits three broad absorptions. These bands are uncharacteristic of the metal ion, as the lowest energy ligand-field states for N_4O_2 coordination in Cr^{III} are invariably found to occur in the visible. These features therefore likely arise from intraligand transitions of the semiquinone or are charge-transfer in nature. On the basis of the observation of similar bands in the spectrum of $[Zn(CTH)(3,5\text{-DTBSQ})]^+$,[43] a compound for which no charge-transfer bands are likely, we assign these bands as $\pi^* \leftarrow$ n intraligand transitions of the coordinated 3,6-DTBSQ.

Region 3. The most intense feature in the visible spectrum of $[Cr(tren)(3,6\text{-DTBSQ})]^{2+}$ is found at 460 nm. The molar extinction coefficient of nearly 6000 M^{-1} cm^{-1} suggests a charge-transfer band, e.g., a ^{3}MLCT $\leftarrow {}^3B_1$ transition. Such an assignment is supported by the observation of a similar band in $[Co(tren)(3,6\text{-DTBSQ})]^{2+}$.[57] In addition, Benelli et al.[46] reported the spectra of both $[Cr(CTH)(TCSQ)]^{2+}$ and $[Cr(CTH)(3,5\text{-DTBSQ})]^{2+}$. A feature similar to that observed in $[Cr(tren)(3,6\text{-DTBSQ})]^{2+}$ is shifted to the red in the tetrachloro complex relative to the alkyl-substituted semiquinone. Given the more positive reduction potential of the tetrachlorosemiquinone, a bathochromic shift of a MLCT band is to be expected for the TCSQ complex. However, the fact that this band in all of the Cr^{III} complexes mentioned above is so narrow makes such an assignment somewhat troubling. The potential energy surface associated with the MLCT state should be displaced relative to the ground state given its formal composition as a Cr^{IV}−catechol species, thus giving rise to a broad absorption band. This notion, coupled with the lack of any significant solvatochroism,[71] therefore casts some doubt on the validity of a CT assignment.

One possibility is that the band at 460 nm is another exchange-enhanced ligand-field band, perhaps associated with the $^2T_{2g}$ octahedral term (see caption, Figure 7). We note that the higher-energy features in the spectrum (i.e., $\lambda < 450$ nm) respond somewhat more to changes in solvent than do any of the other bands in the spectrum, suggesting that either they are charge-transfer in character or they are possibly obscuring a broader band that is solvatochromic. If intensity stealing is in part responsible for the large oscillator strengths of the exchange-enhanced absorptions, then the increased intensity of the 460 nm band relative to the 665 nm bands could be a simple consequence of their relative proximity to charge-transfer transitions in the blue and near-ultraviolet regions of the spectrum. As with other bands in the spectrum, definitive assignments for these features will be afforded by the single-crystal work currently underway.[70]

Excited-State Spectroscopy. Insight into the effect exchange coupling has on excited-state properties can be gained from static emission as well as time-resolved emission and absorption spectroscopies. Again, we choose as our baseline the photophysics of the catecholate complex. In Figure 8 is shown the static emission spectrum of $[Cr(tren)(3,6\text{-DTBCat})](PF_6)$ in a 4:1 EtOH/MeOH glass at 90 K. The spectrum shows a strong band at 725 nm, with several weaker satellites tailing off into the red. Assigning the nature of the emissive state of Cr^{III} complexes can sometimes be ambiguous, particularly for low-symmetry molecules in which the lowest-energy state is not necessarily of ^{2}E parentage.[41] For example, a strongly tetragonal ligand field can cause a low-symmetry component of the $^2T_1$ state ($^2E^Q$, in accord with Forster's nomenclature[41]) to drop below the ^{2}E state in energy. Alternatively, a sufficiently weak ligand field can result in the $^4T_2$ state being lowest in energy, thereby giving rise to prompt fluorescence as opposed to the longer-lived phosphorescence characteristic of a $\Delta S = 1$ transition. Several factors must therefore be taken into account before an assignment can be made with reasonable certainty.

In the case of $[Cr(tren)(3,6\text{-DTBCat})]^+$, however, the spectrum exhibits many characteristics typical of classic, ^{2}E-based emission. Most obvious is the narrow spectral bandwidth, indicative of an intraconfigurational transition and relatively little displacement between the excited- and ground-state potential energy surfaces. This fact coupled with the observed lifetime (vide infra) clearly rules out a $^4T_2 \rightarrow {}^4A_2$ type of fluorescence

(70) Wheeler, D. E.; Zink, J. I.; McCusker, J. K. Unpublished results.

(71) Variable solvent studies have been carried out on this complex as well, but no significant spectral shifting is observed.

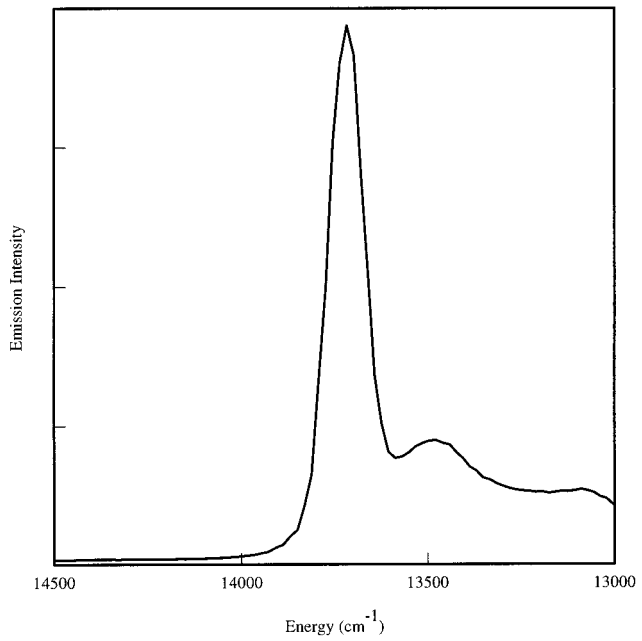

Figure 8. Emission spectrum of [Cr(tren)(3,6-DTBCat)](PF_6) in a 4:1 EtOH/MeOH glass at 90 K.

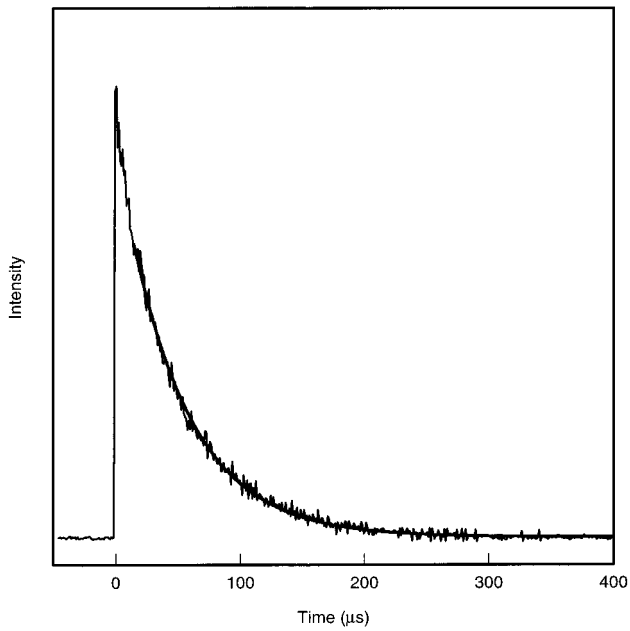

Figure 9. Time-resolved emission decay for [Cr(tren)(3,6-DTBCat)]-(PF_6) at 760 nm following excitation at 425 nm. The smooth solid line is a fit to a single-exponential decay with $k_{obs} = 1.98 \pm 0.05 \times 10^4$ s^{-1}.

as an assignment. The two remaining possibilities for spin-forbidden transitions are of $^2T_1$ or ^2E parentage. Emission from low-symmetry components of the $^2T_1$ state have been assigned for several *trans*-CrN_4F_2 systems, e.g., $[Cr(phen)_2F_2]^+$.[72] In these complexes, the strong tetragonal ligand field gives rise to a state inversion in which the $^2E^Q$ component of the $^2T_1$ state drops below the octahedral-based ^2E state. Although the ligand-field symmetry of $[Cr(tren)(3,6\text{-DTBCat})]^+$ is low, the differences in ligand-field strength along the various bond axes do not qualify as the type of strong tetragonal distortion in which state inversion has been observed in other systems. In addition, the spectra of complexes for which state inversion has been proposed are generally broad due to the ligand-field-dependent nature of the $^2E^Q$ state;[73,74] the sharpness of the spectrum in Figure 8 is inconsistent with this type of an assignment. Finally, the overall spectral profile shown in Figure 8 is very similar to those of several other closely related complexes such as $[Cr(en)_2(H_2O)_2]^{3+}$ for which $^2E \rightarrow {}^4A_2$ assignments have been made.[75] We therefore ascribe emission in [Cr(tren)(3,6-DTBCat)]$^+$ as arising from one (or both) of the $^2A_1$ state(s) derived from the lowest-energy octahedral ^2E state as shown in Figure 7.

Two other aspects concerning the emission spectrum of $[Cr(tren)(3,6\text{-DTBCat})]^+$ should be mentioned. The first is that the emission maximum of 725 nm is significantly red-shifted from the range 660−700 nm typically observed for ^2E-based emission in Cr^{III} complexes. For example, $[Cr(en)_2(ox)]^+$ emits at 685 nm,[41] and other closely related compounds such as $[Cr(en)_2(H_2O)_2]^{3+}$,[75] *cis*-$[Cr(NH_3)_4(H_2O)_2]^{3+}$,[76] and *cis*-$[Cr(cyclam)(H_2O)_2]^{3+}$ [77] all exhibit emission maxima in the 665−695 nm range in alcoholic solution at 77 K. The observed red shift in $[Cr(tren)(3,6\text{-DTBCat})]^+$ can be accounted for by a nephelauxetic effect due to the catechol acting as a π-acceptor. Overlap between the d-orbitals of the metal and the empty π^* orbital(s) of the catechol will result in partial delocalization of the d-electrons onto the ligand. The concomitant reduction in electron−electron repulsion will lower the energy of the ^2E state,[41] thereby causing a red shift in the emission maximum. Similar effects have been observed in other compounds containing π-acceptor ligands: emission from $[Cr(CN)_6]^{3-}$, for example, is observed near 800 nm.[78]

The second point concerns the structure observed in the emission spectrum. With the $^2A_1 \rightarrow {}^4A_1$ assignment given above, it is tempting to ascribe the most intense peak at 725 nm to the electronic origin, and the low-energy bands to a vibronic progression of this 0−0 transition. However, examination of the spacings of these bands does not support such an assignment: the difference in energy between the 725 nm band and the first sideband is 240 cm^{-1}, whereas the second sideband is 390 cm^{-1} from the first band. This is inconsistent with a simple progression of a single vibrational mode, but may reflect a superposition of progressions along several modes. Since the precise origin of these features is not germane to the present discussion of exchange effects, we will not pursue this point further at this time.[79]

In addition to static emission spectra, we have also carried out time-resolved emission studies of $[Cr(tren)(3,6\text{-DTBCat})]^+$. A representative decay trace is illustrated in Figure 9. The observed lifetime of 50 μs is consistent with excited-state lifetimes observed for similar compounds, e.g., *cis*-$[Cr(en)_2(H_2O)_2]^{3+}$ ($\tau_{obs} = 62$ μs),[75] *cis*-$[Cr(en)_2(OH)_2]^+$ ($\tau_{obs} = 34$ μs),[75] and *cis*-$[Cr(cyclam)(H_2O)_2]^{3+}$ ($\tau_{obs} = 74$ μs).[77] The fit to a single-exponential decay is quite good, indicating that any environmental inhomogeneities associated with the glass matrix are having little or no effect on the observed lifetime.

(72) Glerup, J.; Monsted, O.; Schäffer, C. E. *Inorg. Chem.* **1976**, *15*, 1399.
(73) Fucaloro, A. F.; Forster, L. S.; Glover, S. G.; Kirk, A. D. *Inorg. Chem.* **1985**, *24*, 4242.
(74) Ghaith, A. M.; Forster, L. S.; Rund, J. V. *Inorg. Chem.* **1987**, *26*, 2493.
(75) Forster, L. S.; Rund, J. V.; Fucaloro, A. F.; Lin, S. H. *J. Phys. Chem.* **1984**, *88*, 5017.
(76) Fucaloro, A. F.; Forster, L. S.; Rund, J. V.; Lin, S. H. *J. Phys. Chem.* **1983**, *87*, 1796.
(77) Forster, L. S.; Monsted, O. *J. Phys. Chem.* **1986**, *90*, 513.
(78) Ghaith, A.; Forster, L. S.; Rund, J. V. *Inorg. Chim. Acta* **1986**, *16*, 11.
(79) We are currently engaged in variable-temperature emission studies to further elucidate the details of the excited-state properties of this system and will be reporting the results of this work elsewhere.

We attempted to carry out analogous measurements on [Cr(tren)(3,6-DTBSQ)]$^{2+}$ in order to assess the effect of exchange interactions on excited-state decay kinetics. On the basis of the change in extinction coefficient of the formally $^4A_1 \rightarrow {}^2A_1$ absorption upon introduction of excited-state exchange (Figures 5b and 7), we can anticipate an increase in the rate of radiative decay from this lowest energy ligand-field state of approximately 3−4 orders of magnitude for [Cr(tren)(3,6-DTBSQ)]$^{2+}$ relative to the catecholate. However, we were unable to observe any emission from [Cr(tren)(3,6-DTBSQ)]$^{2+}$ in 4:1 EtOH/MeOH at 90 K in the range 500−850 nm, nor at 77 K when probed out to 1400 nm. Furthermore, no emission was observed from a single crystal of this complex at 10 K following excitation at 480 nm.[70] The radiative quantum yield from a state *i*, Φ_r, is given by

$$\Phi_r = \frac{\sum(k_r)_i}{\sum(k_r)_i + \sum(k_{nr})_i} \qquad (3)$$

where $\sum(k_r)_i$ and $\sum(k_{nr})_i$ are the sums of all radiative and nonradiative rates of decay from state *i*, and $k_{obs} = \tau_{obs}{}^{-1} = [\sum(k_r)_i + \sum(k_{nr})_i]$. Given that our detection threshold for emission corresponds to a quantum yield of the order of 10^{-3}−10^{-4}, we can infer that the nonradiative rate constant for decay from the lowest-energy ligand-field state of [Cr(tren)(3,6-DTBSQ)]$^{2+}$ must have increased by a factor of at least 10^7 relative to [Cr(tren)(3,6-DTBCat)]$^+$ in order to account for the lack of emission.

Since time-resolved emission cannot be used to study [Cr(tren)(3,6-DTBSQ)]$^{2+}$, we sought to use time-resolved absorption spectroscopy to try and elucidate details about excited-state dynamics in the semiquinone complex. However, excitation at a number of different absorption wavelengths of a solution of [Cr(tren)(3,6-DTBSQ)]$^{2+}$ at room temperature failed to produce any transient signals in the 400−700 nm probe region. We believe this is indicative of a sub-nanosecond lifetime for the excited state(s) of this complex at room temperature. Such a result would be wholly consistent with the lack of emission from this compound at lower temperatures, considering that the rate of nonradiative decay will most likely increase with increasing temperature. We are currently engaged in both low-temperature nanosecond as well as femtosecond absorption experiments on this compound in order to detail its excited-state dynamics (vide infra).

Concluding Comments

This paper is the first installment from our lab on the photophysics of exchange-coupled compounds. Our goal was to document the synthetic, structural, electronic, and optical characteristics of Cr^{III}−quinone dyads, a compositional motif we believe represents an excellent paradigm for the systematic study of the effect of electron exchange on the photoinduced properties of metal complexes. We have demonstrated a facile, general route into these complexes, as well as provided the first structurally characterized example of a Cr^{III}−monosemiquinone complex. Magnetic susceptibility data confirm the expected presence of a strong anitferromagnetic exchange interaction between the metal and the semiquinone ligand, and a qualitative ligand-field theory analysis of the electronic structures of both the semiquinone and catecholate complexes that includes the effects of electronic exchange enables us to account for some of the remarkable optical properties of the exchange-coupled semiquinone complex.

Much of our current research efforts are now focusing on the excited-state dynamics of these complexes, and some initial results from these studies have been presented in this paper. While the catecholate complex exhibits emissive properties characteristic of classic, ^2E-based Cr^{III} excited-state decay, the semiquinone analogue does not emit even as a single crystal at 10 K. This lack of emission in [Cr(tren)(3,6-DTBSQ)]$^{2+}$ coupled with the pronounced increase in the compound's absorption cross section is indicative of substantial changes in both radiative and nonradiative excited-state decay processes upon oxidation of the catecholate complex. It is tempting to attribute these changes in excited-state decay dynamics to the introduction of electron exchange into the ground- and excited-state electronic manifolds of the complex. Given the marked perturbation in electronic structure that electron exchange induces (see Figure 7), a correspondingly large change in the dynamics of excited-state relaxation would not be surprising. However, the presence of low-lying, ligand-based absorptive features in the spectrum of [Cr(tren)(3,6-DTBSQ)]$^{2+}$ necessitates that caution be exercised before such a correlation is made. The lack of emission in this particular complex could simply be a manifestation of Kasha's rule, with the inferred increase in k_{nr} being a reflection of rapid depopulation of the $^2A_1$ state(s) in favor of these lower energy ligand-localized states. A key challenge, then, is distinguishing between this possibility and the effects of electron exchange that we wish to explore. One virtue of the present system is its inherent synthetic flexibility, making it possible to manipulate the electronic structures of these compounds with relative ease. Such compositional variations coupled with low-temperature and short time scale measurements (e.g., femtosecond time-resolved absorption spectroscopy) should allow for differentiating between changes in excited-state dynamics due to low-lying ligand-localized electronic states and effects due to electron exchange interactions.

Acknowledgment. The authors would like to thank Juanita Wickham and Professor Paul Alivisatos for assistance with the near-IR emission experiment and Professor Jeff Zink for the low-temperature single-crystal measurements. This work was supported by the National Science Foundation (CHE-9729003).

Supporting Information Available: Tables of positional parameters, anisotropic displacement factors, and extended tabulations of bond distances, angles, and nonbonded contacts (8 pages). Ordering information is given on any current masthead page.

IC971306I